

Engineering drag currents in Coulomb coupled quantum dots

Jong Soo Lim,¹ Rosa López,² and David Sánchez²

¹*School of Physics, Korea Institute for Advanced Study, Seoul 130-722, Korea*

²*Institut de Física Interdisciplinària i de Sistemes Complexos IFISC (CSIC-UIB), E-07122 Palma de Mallorca, Spain*

The Coulomb drag phenomenon in a Coulomb-coupled double quantum dot system is revisited with a minimal model. Previously, cotunneling effects on the drag current in mesoscopic setups have been reported both theoretically and experimentally. However, in both cases the sequential tunneling contribution was always present in the current detection unless the drag level position were too far away from resonance. Here, we consider the case of very large Coulomb interaction between the dots, whereby the drag current is only driven by cotunneling events. As a consequence, a purely quantum coherent drag effect takes place. Further, we demonstrate that by properly engineering the tunneling probabilities using band tailoring it is possible to control the sign of the drag and drive currents, allowing them to flow in parallel or antiparallel directions. We also report an additional control over the sign of the drag current that can be achieved by varying the drag gate potential.

Introduction.—In a system made of two nearby (electrically) isolated conductors where particles are prevented from tunneling into each other, a bias drop through one conductor can drag a current through the other conductor due to Coulomb interaction between them [1, 2]. The Coulomb drag effect was first suggested by Pogrebinskii [3] and Price [4] theoretically and explained by energy and momentum transfer from the drive conductor to the drag conductor due to Coulomb mutual friction. This phenomenon has become a quite useful toolbox to probe electron-electron or electron-hole scattering mechanisms in many-body systems. At the early stage, the effect has been observed in semiconductor 2D-3D electron gas layers [5], 2D-2D electron gas layers [6], 2D electron gas-2D hole gas layers [7] and then investigated under the influence of a perpendicular magnetic field [8–17]. Since the Coulomb interaction is stronger in 1D than 2D, Coulomb drag between 1D-1D quantum nanowires has been also extensively explored [18–21]. More recently, interest has shifted to more exotic systems such as graphene double layers [22–24], graphene double ribbons [25], graphene-2D electron gases [26], or double bilayer graphene heterostructures [27]. In addition, Coulomb drag between quantum wire and quantum dot [28], between quantum dots [29], or between quantum point contacts [30] has been demonstrated. In such systems translational symmetry is broken. Hence, Coulomb drag effect assisted by momentum transfer is no longer possible and only energy transfer between the two subsystems takes place. Energy exchange between the drive and drag subsystems leads to rectification of nonequilibrium fluctuations [31] in close analogy to the ratchet effect [32, 33] with possible energy harvesting applications [34].

Reducing the dimensionality of nanoscale devices has a two-fold advantage, namely: (i) the Coulomb interaction enhances by diminishing the system size system, which leads to a major dragging effect; (ii) a very small drive voltage yields a drag current generated by the excess of noise of the drive system. Both properties may play sig-

nificant roles in quantum information processing. Enhanced Coulomb interaction can entangle particles in a controlled way while drag currents can be used for quantum measurement purposes, where the drag subsystem serves as the detector. In this context, drag currents can be regarded as the back-action resulting from quantum measurements in the drive system. Importantly, these systems exhibit quantum coherence. Here, we demonstrate that quantum coherence is crucial in the strongly interacting mesoscopic Coulomb drag effect.

Reference 35 proposes a simple mesoscopic setup that consists of two parallel Coulomb-coupled quantum dots attached to four separate normal electron reservoirs to generate the Coulomb drag current. Using this device, it is possible to test fundamental fluctuation relations among nonlinear transport coefficients. Both quantum dots are very closely spaced so that a very strong interdot Coulomb interaction is expected and the setup is thus a natural platform to observe Coulomb drag. Interdot tunneling is forbidden. The setup is analyzed employing the master equation approach, considering only sequential tunneling rates. Dot charge-state dependent tunnel barriers are key ingredients in the prediction of unidirectional drag currents, independently of the direction of the drive bias drop. A recent experiment [36] realizes the setup using a lithographically patterned AlGaAs/GaAs heterostructure and detects unidirectional drag currents as anticipated. However and in contrast to the theory of Ref. [35], the experiment shows at very low temperatures the importance of including cotunneling processes, as demonstrated with a theoretical model that shows excellent agreement with the experimental data [36]. The role of cotunneling processes is also emphasized in Ref. 37 where a similar system is considered but with graphene reservoirs instead of normal electron reservoirs [38]. In both cases, a four-charge state model within a master equation description serves as a theoretical basis to describe the Coulomb drag effect. It is proven that nonlocal cotunneling processes contribute to the drag current to the same order as sequential tunneling events, the for-

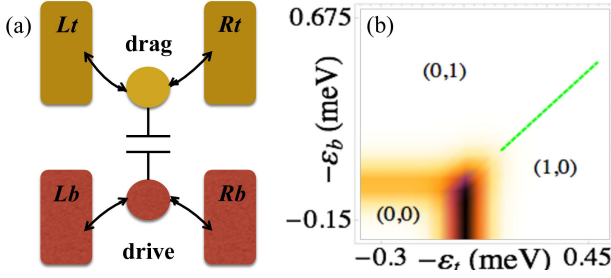


FIG. 1. (a) Sketch of our device. Top dot acts as the drag subsystem held at equilibrium whereas an electrical current is driven across the bottom dot (the drive subsystem). Both dots are tunnel connected to reservoirs as indicated. Coulomb interaction between the two dots (here, represented with a capacitor) is necessary for the drag effect to happen. (b) Stability diagram as a function of the dot top level (ε_t) and the bottom dot level (ε_b). Dot occupations are denoted with (n_t, n_b) . The borders between regions with constant occupations are given by conductance values. In the limit of strong interdot interactions, there exists a unique triple point where charge fluctuations among the states $(0,0) \rightleftharpoons (0,1) \rightleftharpoons (1,0)$. The dotted line is for eye-guiding purposes.

mer being the main contribution when the dot level for the drag subsystem lies well far away from the resonant condition. In such situation, the drag current is mainly driven by high-order tunneling processes. Nevertheless, both analyses also had to take into account sequential processes for a proper description of the drag effect.

Our aim here is to propose a minimal model that totally suppresses sequential tunneling drag currents, leading to a drag effect mainly driven by cotunneling processes. In our setup, the mutual Coulomb interaction is considered to be sufficiently large to discard the double occupation charge state. Therefore, only three charge states are needed to generate and detect drag currents. This is the minimum configuration unlike the four states employed in previous works [35–37]. Based on this model, we will show that the behavior and sign of the mesoscopic drag current can be controlled externally by engineering properly the energy dependence of the tunneling barriers. The system under consideration is plotted in Fig. 1(a). Two parallel coupled quantum dots are attached to four normal electronic reservoirs. Particle flow is indicated with arrows while electron-electron interaction occurs between the dots only (the reservoirs are assumed to be massive electrodes with good screening properties). The stability diagram for this setup is shown in Fig. 1(b). The diagram is obtained by summing the linear conductances $G_i = (dI_i/dV_i)_{V_i=0}$ ($i = t, b$) through the drag (top, t) and drive (bottom, b) dots and plotted as a function of the top (ε_t) and the bottom (ε_b) gate voltages. Here, $I_i(V_i)$ is the current (voltage) across the subsystem $i = t, b$ and (n_t, n_b) denotes the dot charge configurations, where n_t and n_b are the number of electrons on dot t and b . When the Coulomb interaction strength is very large the

resulting stability diagram shown in Fig. 1(b) displays only one triple point where the doubly occupied configuration $(1,1)$ never takes place, $(1,0)$ and $(0,1)$ being equally probable.

Theory.—The model Hamiltonian has three contributions, i.e., $\mathcal{H} = \mathcal{H}_D + \mathcal{H}_C + \mathcal{H}_T$. $\mathcal{H}_D = \sum_{i=t/b} \varepsilon_i d_i^\dagger d_i + U d_t^\dagger d_t d_b^\dagger d_b$ describes the quantum dots. The operator d_i^\dagger (d_i) creates (annihilates) an electron with energy ε_i on the dot i . The interdot charging energy is denoted with U . By adjusting gate voltages appropriately, the direct tunneling between quantum dots is forbidden and can be safely neglected [36]. $\mathcal{H}_C = \sum_{\alpha=L/R, i, k} \varepsilon_{\alpha ik} c_{\alpha ik}^\dagger c_{\alpha ik}$ depicts the reservoir Hamiltonian where $c_{\alpha ik}^\dagger$ ($c_{\alpha ik}$) creates (annihilates) an electron with wavevector k and energy $\varepsilon_{\alpha ik}$ in the reservoir $\alpha i = \{Lt, Lb, Rt, Rb\}$ [Fig. 1(a)]. $\mathcal{H}_T = \sum_{\alpha, i, k} (t_{\alpha ik} c_{\alpha ik}^\dagger d_i + \text{H.c.})$ characterizes the coupling between the top and bottom dots and the reservoirs via the tunneling amplitudes $t_{\alpha ik}$.

We focus on the dot states, tracing out the reservoir degrees of freedom. In our system and for $U \rightarrow \infty$, there are three possible dot states $|n\rangle = \{|0\rangle, |t\rangle, |b\rangle\}$. The state $|0\rangle \equiv (0,0)$ implies that both dots are empty, while $|t\rangle \equiv (1,0)$ ($|b\rangle \equiv (0,1)$) indicates that the top (bottom) dot is occupied. To lowest order in \mathcal{H}_T , the transition (sequential tunneling) rate from $|m\rangle$ to $|n\rangle$ entering or leaving the reservoir αi is given by [39] $\mathcal{W}_{mn}^{\alpha i} = \frac{2\pi}{\hbar} \text{Tr}_C [F_{mC} |\langle n | \langle n | \mathcal{H}_T \mathcal{G}_0 \mathcal{H}_T | m \rangle | m_C \rangle|^2] \delta(E_m + E_{mC} - E_n - E_{nC})$ where Tr_C designates a trace over the reservoir degrees of freedom, F_{mC} is the thermal distribution function for the reservoir state m_C with energy E_{mC} , and E_m and E_n are the energies of the states $|m\rangle$ and $|n\rangle$. The second-order rate in \mathcal{H}_T describes the cotunneling processes from $|m\rangle$ to $|n\rangle$ and is calculated as

$$\gamma_{mn}^{\alpha i \beta j} = \frac{2\pi}{\hbar} \text{Tr}_C [F_{mC} |\langle n | \langle n | \mathcal{H}_T \mathcal{G}_0 \mathcal{H}_T | m \rangle | m_C \rangle|^2] \times \delta(E_m + E_{mC} - E_n - E_{nC}), \quad (1)$$

where \mathcal{G}_0 is the resolvent operator given by $\mathcal{G}_0 = \frac{1}{E_m - \mathcal{H}_0}$ with $\mathcal{H}_0 = \mathcal{H}_D + \mathcal{H}_C$. Conceptually, one might go further by including higher-order tunneling processes in \mathcal{H}_T but this is out of the scope of the present work. Our goal is to consider quantum coherent processes to leading order. This approximation is valid provided that the background temperature is not very low ($k_B T > \Gamma_0$, where Γ_0 is the tunnel barrier strength energy to be specified below).

Let P_n be the probability for the state $|n\rangle$. Within the master equation approach, we can write

$$\frac{d}{dt} P_0 = -(\mathcal{W}_{0t} + \mathcal{W}_{0b}) P_0 + \mathcal{W}_{t0} P_t + \mathcal{W}_{b0} P_b, \quad (2a)$$

$$\frac{d}{dt} P_t = \mathcal{W}_{0t} P_0 - (\mathcal{W}_{t0} + \gamma_{tb}) P_t + \gamma_{bt} P_b, \quad (2b)$$

$$\frac{d}{dt} P_b = \mathcal{W}_{0b} P_0 + \gamma_{tb} P_t - (\mathcal{W}_{b0} + \gamma_{bt}) P_b, \quad (2c)$$

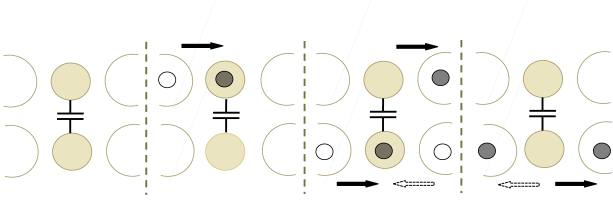


FIG. 2. Characteristic transport sequence involving a cotunneling process. Empty (filled) circles represent electrons leaving (arriving at) the different parts of the system (reservoirs or dots). Arrows indicate the transport direction. Due to the applied bias, right going processes in the drive subsystem (filled arrows) dominate over left going transitions (dashed arrows). While the second and four processes are sequential, the third process is a purely cotunneling event.

where $\mathcal{W}_{mn} = \sum_{\alpha i} \mathcal{W}_{mn}^{\alpha i}$ and $\gamma_{mn} = \sum_{\alpha i, \beta j} \gamma_{mn}^{\alpha i \beta j}$. Importantly, the singly occupied states $|t\rangle$ and $|b\rangle$ are interconnected thanks to the cotunneling rates. In contrast, sequential tunneling processes always involve the empty state $|0\rangle$.

The stationary probabilities (st) can be obtained from Eq. (2) in the limit $t \rightarrow \infty$ with the aid of the probability conservation law $\sum_n P_n = 1$. Therefore, we can focus on the current flowing into the left top (Lt) reservoir ($I_{\text{drag}} \equiv I_{Lt}$),

$$I_{\text{drag}} = -e [\mathcal{W}_{0t}^{Lt} P_0^{\text{st}} - (\mathcal{W}_{t0}^{Lt} + \gamma_{tb}^{LbLt} + \gamma_{tb}^{RbLt}) P_t^{\text{st}} + (\gamma_{bt}^{LtLb} + \gamma_{bt}^{LtRb}) P_b^{\text{st}}], \quad (3)$$

where e denotes the elementary positive electric charge. Crucially, when cotunneling processes are neglected the drag current identically vanishes and the doubly occupied state must be then considered. Nonzero cotunneling rates allow the charge configuration space to be reduced to just three states.

On the other hand, the drive current ($I_{\text{drive}} \equiv I_{Lb}$) is

$$I_{\text{drive}} = -e [(\mathcal{W}_{0b}^{Lb} - \gamma_{00}^{RbLb} + \gamma_{00}^{LbRb}) P_0^{\text{st}} + (\gamma_{tb}^{LbLt} + \gamma_{tb}^{LbRt}) P_t^{\text{st}} - (\mathcal{W}_{b0}^{Lb} + \gamma_{bb}^{RbLb} - \gamma_{bb}^{LbRb} + \gamma_{bt}^{LtLb} + \gamma_{bt}^{RtLb}) P_b^{\text{st}}]. \quad (4)$$

Unlike Eq. (3), Eq. (4) can be nonzero if the γ 's are nullified since a voltage is present in the drive subsystem.

Calculating the sequential tunneling rates explicitly [40], we find $I_{\text{drag}}^{(\text{seq})} \propto \Gamma_{Lt}(\varepsilon_t) \Gamma_{Rt}(\varepsilon_t) [f_{Rt}(\varepsilon_t) - f_{Lt}(\varepsilon_t)] \sum_{\alpha} \Gamma_{\alpha b}(\varepsilon_b) [1 - f_{\alpha b}(\varepsilon_b)]$ where $f_{\alpha i}(\varepsilon) = 1/[1 + e^{(\varepsilon - \mu_{\alpha i})/k_B T}]$ is the Fermi function to be evaluated using an electrostatic model [40] with $\mu_{\alpha i}$ the electrochemical potential of lead αi . The hybridization widths $\Gamma_{\alpha i}(\varepsilon) = 2\pi \sum_k t_{\alpha i k}^2 \delta(\varepsilon_{\alpha i k} - \varepsilon) = 2\pi t_{\alpha i}^2(\varepsilon) \rho_{\alpha i}(\varepsilon)$ depend on the tunnel amplitude $t_{\alpha i}$ and density of states (DOS) $\rho_{\alpha i}$. Since $\mu_{Lt} = \mu_{Rt}$ in the drag system, we take $f_{Lt}(\varepsilon) = f_{Rt}(\varepsilon) \equiv f_t(\varepsilon)$ leading to a zero drag current

in the sequential tunneling regime when $U \rightarrow \infty$. Consider now what happens when we include cotunneling processes. The sequence $|0\rangle \rightarrow |t\rangle \rightarrow |b\rangle \rightarrow |0\rangle$ is illustrated in Fig. 2, where an electron is transported from left to right in the drag subsystem. The corresponding probability is proportional to $\mathcal{W}_{0t}^{Lt} \gamma_{tb}^{\alpha b Rt} \mathcal{W}_{b0}^{\beta b}$. The probability for the reversed process reads $\mathcal{W}_{0t}^{Rt} \gamma_{tb}^{\alpha b Lt} \mathcal{W}_{b0}^{\beta b}$. As a consequence, the net current becomes $I_{\text{drag}} \propto \sum_{\alpha, \beta} (\mathcal{W}_{0t}^{Lt} \gamma_{tb}^{\alpha b Rt} \mathcal{W}_{b0}^{\beta b} - \mathcal{W}_{0t}^{Rt} \gamma_{tb}^{\alpha b Lt} \mathcal{W}_{b0}^{\beta b})$, which in terms of the explicit expressions for the tunneling rates [41, 42] we have

$$I_{\text{drag}} \propto \sum_{\alpha, \beta} \int d\varepsilon \left| \frac{1}{\varepsilon - \varepsilon_b} \right|^2 [\Gamma_{Lt}(\varepsilon_t) \Gamma_{Rt}(\varepsilon + \varepsilon_t - \varepsilon_b) - \Gamma_{Rt}(\varepsilon_t) \Gamma_{Lt}(\varepsilon + \varepsilon_t - \varepsilon_b)] \Gamma_{\alpha b}(\varepsilon) \Gamma_{\beta b}(\varepsilon_b) \times f_t(\varepsilon_t) f_{\alpha b}(\varepsilon) [1 - f_t(\varepsilon + \varepsilon_t - \varepsilon_b)] [1 - f_{\beta b}(\varepsilon_b)]. \quad (5)$$

Clearly, I_{drag} vanishes when $\Gamma_{\alpha i}(\varepsilon) = \Gamma_{\alpha i}$ and thus energy-dependent tunnel barriers are needed.

We envisage that one of the tunnel barriers (top left, Lt) has a Lorentzian profile,

$$\Gamma_{Lt}(\varepsilon) = \frac{\Gamma_{Lt}}{1 + [(\varepsilon - \mu_{Lt})/D]^2}, \quad (6)$$

and the other tunnel barriers are constant, i.e., $\Gamma_{Rt}(\varepsilon) = \Gamma_{Rt}$, $\Gamma_{Lb}(\varepsilon) = \Gamma_{Lb}$, $\Gamma_{Rb}(\varepsilon) = \Gamma_{Rb}$. This model can be realized with constant tunnel amplitudes ($t_{\alpha i}(\varepsilon) = t_{\alpha i}$) while the DOS for the left top reservoir $\rho_{Lt}(\varepsilon)$ is Lorentzian and the other reservoirs have flat bands. Tailoring of the band structure in the leads can be achieved with different materials [43]. In the following we present our results for the drive and drag currents and discuss the tunability of the drag current depending on the system parameters.

Results.—Throughout this paper, we take $\Gamma_{Lt} = \Gamma_{Rt} = (47/15)\Gamma_0$ and $\Gamma_{Lb} = \Gamma_{Rb} = \Gamma_0$ where $\Gamma_0 = 7.5 \mu\text{eV}$ is the unit of energy. These values were extracted from the experiment [36]. The temperature is set to $k_B T = 5\Gamma_0$ and $D = 10\Gamma_0$. We evaluate the drag (I_{drag}) and drive (I_{drive}) currents as a function of ε_t and ε_b for a drive voltage $V_b \neq 0$. In Figs. 3(a) and (b), we observe that I_{drag} is strongest along the (green) dotted line shown in Fig. 1(b). Therefore, drag currents are intimately related to charge fluctuations since $I_{\text{drag}} \neq 0$ for the sequence depicted in Fig. 2, in which case the three states $|0\rangle$, $|t\rangle$, $|b\rangle$ have similar probabilities and as a consequence I_{drag} is maximal around the triple point in Fig. 1(b). Reversing the direction of V_b does not change the direction of I_{drag} but merely shifts the drag regions down following the bias window [36]. Surprisingly enough, unlike the experimental results [36] our drag current changes sign when ε_t is tuned. The phenomenon is illustrated in Fig. 4. When $\varepsilon_t > \mu_L$ (left panel) thermally excited

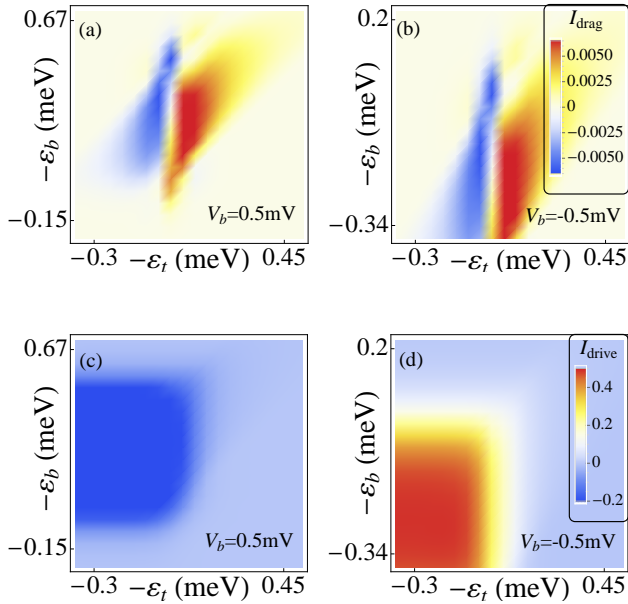


FIG. 3. Drag current I_{drag} (top panels) and drive current I_{drive} (bottom panels) as a function of top (ε_t) and bottom (ε_b) dot level positions. The applied drive bias voltage is $V_b = 0.5$ mV (a,c) and $V_b = -0.5$ mV (b,d). Current is expressed in units of $e\Gamma_0/h$.

electrons from the left reservoir can tunnel to the right lead and a negative current is then obtained (our flux sign convention states that the current is negative when it leaves the reservoir). If $\varepsilon_t < \mu_L$ (right panel) the I_{drag} direction is reversed because electrons below the Fermi energy in the right lead tend to fill the available states in the left reservoir, thus creating hole-like transport. Obviously, for $\varepsilon_t = \mu_L$ (middle panel) electron- and hole-like fluxes compensate each other and the net current is zero [see the border line between the blue and red regions in Fig. 3(a,b)]. The discussed effect implies that we can engineer I_{drag} by the gate voltage tuning ε_t with a suitable model for the electronic DOS at the reservoirs. This is a central prediction of our work. Incidentally, the region in which there is an appreciable drag current is extended to ε_t values far away from resonance. This is due only to cotunneling processes since a purely sequential model yields sharp boundaries [35].

In Figs. 3(c) and (d) we plot the drive current as a function of the level position for a nonzero V_b . For $V_b > 0$ ($V_b < 0$) the current is negative (positive), as expected. In both cases the current is nonzero only when the ε_b is within the bias window [i.e., when $-eV_b - \varepsilon_b^0 \lesssim \varepsilon_b \lesssim \varepsilon_b^0$ where $\varepsilon_b^0 \simeq 0$ meV signals the transition $(0,0) \rightarrow (0,1)$ in Fig. 1(b)]. Interestingly, I_{drive} also depends on ε_t . This can be understood as follows. When the top dot level falls below the Fermi energy, the drag dot becomes occupied and transport across the drive dot remains blocked due

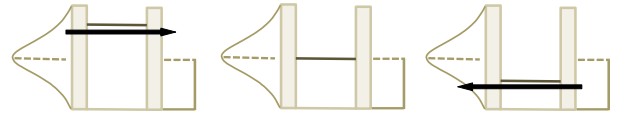


FIG. 4. Sketch of the drag dot for $\mu_{Lt} = \mu_{Rt}$ (dashed lines) and three different level positions (filled dark lines). The left (right) reservoir displays a Lorentzian (flat) density of states, which determines the current direction (long arrows).

to the strong electron-electron interaction between the dots (gating effect). Importantly, for a wide range of ε_t both currents (drag and drive) run in parallel if $V_b > 0$ [cf. Figs. 3(a) and (c)] but flow in antiparallel directions if $V_b < 0$ [cf. Figs. 3(b) and (d)]. This results in an additional degree of tunability by controlling ε_d and V_b independently.

Conclusion.—We considered a three-state model to propose a device for the observation of purely coherent drag effect. The system consists of two parallel quantum dots which are connected electrostatically with an infinite interdot Coulomb interaction. A clever design for the reservoir density of states leads to a powerful tunability for the drive and drag currents. Thus, we illustrated our findings with a model in which the left top coupling has a Lorentzian density profile and the other couplings are constant. We demonstrated that the drag current flows in parallel or in opposite direction when compared with the drive current by reversing the sign of the bias voltage. Further, the drag current changes its sign when the dot energy level is varied with an external gate potential. This is in contrast with the results for finite charging energy models [36, 37] in which the drag current is unidirectional independently of the value of the drive bias voltage. Our proposal opens a new route for the detection and manipulation of coherent drag currents in nanoscale conductors.

Acknowledgments.—This work was supported by MINECO under grant No. FIS2014-52564.

-
- [1] A. G. Rojo, J. Phys.: Condens. Matter **11**, R31 (1999).
 - [2] B. N. Narozhny and A. Levchenko, Rev. Mod. Phys. **88**, 025003 (2016).
 - [3] M. B. Pogrebinskii, Fiz. Tekh. Poluprovodn **11**, 637 (1977) [Sov. Phys.-Semicond. **11**, 372 (1977)].
 - [4] P. J. Price, Physica B **117-118**, 750 (1983).
 - [5] P. M. Solomon, P. J. Price, D. J. Frank, and D. C. La Tulipe, Phys. Rev. B **63**, 2508 (1989).
 - [6] T. J. Gramila, J. P. Eisenstein, A. H. MacDonald, L. N. Pfeiffer, and K. W. West, Phys. Rev. Lett. **66**, 1216 (1991); Phys. Rev. B **47**, 12957 (1993); Physica B **197**, 442 (1994).
 - [7] U. Sivan, P. M. Solomon, and H. Shtrikman, Phys. Rev. Lett. **68**, 1196 (1992).
 - [8] N. P. R. Hill, J. T. Nicholls, E. H. Linfield, M. Pepper,

- D. A. Ritchie, A. R. Hamilton, and G. A. C. Jones, J. Phys.: Condens. Matter **8**, L557 (1996).
- [9] H. Rubel, A. Fischer, W. Dietsche, K. von Klitzing, and K. Eberl, Phys. Rev. Lett. **78**, 1763 (1997).
- [10] M. P. Lilly, J. P. Eisenstein, L. N. Pfeiffer, and K. W. West, Phys. Rev. Lett. **80**, 1714 (1998).
- [11] X. G. Feng, S. Zelakiewicz, H. Noh, T. J. Ragucci, and T. J. Gramila, L. N. Pfeiffer, and K. W. West, Phys. Rev. Lett. **81**, 3219 (1998).
- [12] J. G. S. Lok, S. Kraus, M. Pohl, W. Dietsche, K. von Klitzing, W. Wegscheider, and M. Bichler, Phys. Rev. B **63**, 041305(R) (2001).
- [13] M. Kellogg, I. B. Spielman, J. P. Eisenstein, L. N. Pfeiffer, and K. W. West, Phys. Rev. Lett. **88**, 126804 (2002).
- [14] M. Kellogg, J. P. Eisenstein, L. N. Pfeiffer, and K. W. West, Phys. Rev. Lett. **90**, 246801 (2003).
- [15] K. Muraki, J. G. S. Lok, S. Kraus, W. Dietsche, K. von Klitzing, D. Schuh, M. Bichler, and W. Wegscheider, Phys. Rev. Lett. **92**, 246801 (2004).
- [16] E. Tutuc, R. Pillarisetty, and M. Shayegan, Phys. Rev. B **79**, 041303(R) (2009).
- [17] D. Nandi, A. D. K. Finck, J. P. Eisenstein, L. N. Pfeiffer, and K. W. West, Nature **488**, 481 (2012).
- [18] P. Debray, P. Vasilopoulos, O. Raichev, R. Perrin, M. Rahman, W. C. Mitchel, Physica E **6**, 694 (2000).
- [19] P. Debray, V. Zverev, O. Raichev, R. Klesse, P. Vasilopoulos, and R. S. Newrock, J. Phys.: Condens. Matter **13** 3389 (2001).
- [20] M. Yamamoto, M. Stopa, Y. Tokura, Y. Hirayama, S. Tarucha, Physica E **12**, 726 (2002); Science **313**, 204 (2006).
- [21] D. Laroche, G. Gervais, M. P. Lilly, and J. L. Reno, Nature Nanotechnol. **6**, 793 (2011); Science **343**, 631 (2014).
- [22] S. Kim, I. Jo, J. Nah, Z. Yao, S. K. Banerjee, and E. Tutuc, Phys. Rev. B **83**, 161401(R) (2011).
- [23] R. V. Gorbachev, A. K. Geim, M. I. Katsnelson, K. S. Novoselov, T. Tudorovskiy, I. V. Grigorieva, A. H. MacDonald, S. V. Morozov, K. Watanabe, T. Taniguchi, and L. A. Ponomarenko, Nature Phys. **8**, 896 (2012).
- [24] S. Kim, E. Tutuc, Solid State Commun. **152**, 1283 (2012).
- [25] H. Chen and J. Appenzeller, Nano Res. **6**, 897 (2013).
- [26] A. Gamucci, D. Spirito, M. Carrega, B. Karmakar, A. Lombardo, M. Bruna, L. N. Pfeiffer, K. W. West, A. C. Ferrari, M. Polini, and V. Pellegrini, Nature Commun. **5**, 5824 (2014).
- [27] K. Lee, J. Xue, D. C. Dillen, K. Watanabe, T. Taniguchi, and E. Tutuc, Phys. Rev. Lett. **117**, 046803 (2016).
- [28] M. Shimizu, M. Yamamoto, M. Stopa, M. Honda, S. Tarucha, Physica E **26**, 460 (2005).
- [29] G. Shinkai, T. Hayashi, T. Ota, K. Muraki, and T. Fujisawa, Appl. Phys. Express **2**, 081101 (2009).
- [30] V. S. Khrapai, S. Ludwig, J. P. Kotthaus, H. P. Tranitz, and W. Wegscheider, Phys. Rev. Lett. **99**, 096803 (2007).
- [31] A. Levchenko and A. Kamenev, Phys. Rev. Lett. **101**, 216806 (2008).
- [32] R. D. Astumian, Phys. Rev. Lett. **101**, 046802 (2008).
- [33] V. Moldoveanu and B. Tanatar, Phys. Rev. B **82**, 205312 (2010).
- [34] R. Hussein and S. Kohler, Annalen der Physik **527**, 610 (2015).
- [35] R. Sánchez, R. López, D. Sánchez, and M. Büttiker, Phys. Rev. Lett. **104**, 076801 (2010).
- [36] A. J. Keller, J. S. Lim, D. Sánchez, R. López, S. Amasha, J. A. Katine, H. Shtrikman, and D. Goldhaber-Gordon, Phys. Rev. Lett. **117**, 066602 (2016).
- [37] K. Kaashjerg and A.-P. Jauho, Phys. Rev. Lett. **116**, 196801 (2016).
- [38] D. Bischoff, M. Eich, O. Zilberberg, C. Rössler, T. Ihn, and K. Ensslin, Nano Lett. **15**, 6003 (2015).
- [39] H. Bruus and K. Flensberg, *Many-Body Quantum Theory in Condensed Matter Physics* (Oxford University Press, 2004).
- [40] See Supplementary Material.
- [41] D. Averin, Physica B **194-196**, 979 (1994).
- [42] M. Turek and K. A. Matveev, Phys. Rev. B **65**, 115332 (2002).
- [43] *Handbook of the Band Structure of Elemental Solids*, edited by D. A. Papaconstantopoulos (Plenum, New York, 1986).

Supplemental information: Engineering drag currents in Coulomb coupled quantum dots

CALCULATION OF THE TRANSITION RATES

Sequential tunneling

The sequential tunneling rate from state $|m\rangle$ to state $|n\rangle$ is

$$\mathcal{W}_{mn}^{\alpha i} = \frac{2\pi}{\hbar} \text{Tr}_C [F_{m_C} |\langle n_C | \langle n | \mathcal{H}_T | m \rangle | m_C \rangle|^2] \delta(E_m + E_{m_C} - E_n - E_{n_C}). \quad (\text{S1})$$

The superscript αi indicates that the reservoir αi is involved in the tunneling process. The trace Tr_C is taken over the reservoir degrees of freedom. F_{m_C} denotes the thermal distribution function for the reservoir state $|m_C\rangle$

$$F_{m_C} = \frac{e^{-\beta \mathcal{H}_C}}{\text{Tr}_C [e^{-\beta \mathcal{H}_C}]}. \quad (\text{S2})$$

As an example, we evaluate the rate $\mathcal{W}_{0i}^{\alpha i}$ from $|0\rangle$ to $|i\rangle$. Since the final state is

$$|n\rangle |n_C\rangle = d_i^\dagger c_{\alpha i k} |0\rangle |m_C\rangle, \quad (\text{S3})$$

the rate can be written as

$$\mathcal{W}_{0i}^{\alpha i} = \frac{2\pi}{\hbar} \sum_k \sum_{m_C} \left[F_{m_C} \left| \langle m_C | \langle 0 | c_{\alpha i k}^\dagger d_i d_i^\dagger c_{\alpha i k} | 0 \rangle | m_C \rangle \right|^2 \right] \delta(\varepsilon_{\alpha i k} - \varepsilon_i). \quad (\text{S4})$$

We note that

$$\sum_{m_C} F_{m_C} |\langle m_C | c_{\alpha i k}^\dagger c_{\alpha i k} | m_C \rangle|^2 = f_{\alpha i}(\varepsilon_{\alpha i k}). \quad (\text{S5})$$

Equation (S5) follows from the fact that $c_{\alpha i k}^\dagger c_{\alpha i k}$ can only take the values 0 or 1. Therefore, we obtain

$$\mathcal{W}_{0i}^{\alpha i} = \frac{1}{\hbar} \Gamma_{\alpha i}(\varepsilon_i) f_{\alpha i}(\varepsilon_i), \quad (\text{S6})$$

where

$$\Gamma_{\alpha i}(\varepsilon_i) = 2\pi \sum_k t_{\alpha i k}^2 \delta(\varepsilon_{\alpha i k} - \varepsilon_i). \quad (\text{S7})$$

The sequential tunneling rate from $|i\rangle$ to $|0\rangle$ can be similarly found,

$$\mathcal{W}_{i0}^{\alpha i} = \frac{1}{\hbar} \Gamma_{\alpha i}(\varepsilon_i) [1 - f_{\alpha i}(\varepsilon_i)]. \quad (\text{S8})$$

Cotunneling

The cotunneling rate from $|m\rangle$ to $|n\rangle$ is given by

$$\gamma_{mn}^{\alpha i \beta j} = \frac{2\pi}{\hbar} \text{Tr}_C [F_{m_C} |\langle n_C | \langle n | \mathcal{H}_T \mathcal{G}_0 \mathcal{H}_T | m \rangle | m_C \rangle|^2] \delta(E_m + E_{m_C} - E_n - E_{n_C}). \quad (\text{S9})$$

For energy dependent tunnel broadenings, they become

$$\gamma_{00}^{\alpha i \beta i} = \frac{1}{2\pi\hbar} \int d\varepsilon \left| \frac{1}{\varepsilon - \varepsilon_i + i\eta} \right|^2 \Gamma_{\alpha i}(\varepsilon) \Gamma_{\beta i}(\varepsilon) f_{\alpha i}(\varepsilon) [1 - f_{\beta i}(\varepsilon)], \quad (\text{S10a})$$

$$\gamma_{ii}^{\alpha i \beta i} = \frac{1}{2\pi\hbar} \int d\varepsilon \left| \frac{1}{\varepsilon - \varepsilon_i + i\eta} \right|^2 \Gamma_{\alpha i}(\varepsilon) \Gamma_{\beta i}(\varepsilon) f_{\alpha i}(\varepsilon) [1 - f_{\beta i}(\varepsilon)], \quad (\text{S10b})$$

$$\gamma_{i\bar{i}}^{\alpha \bar{i} \beta i} = \frac{1}{2\pi\hbar} \int d\varepsilon \left| \frac{1}{\varepsilon - \varepsilon_{\bar{i}} + i\eta} \right|^2 \Gamma_{\alpha \bar{i}}(\varepsilon) \Gamma_{\beta i}(\varepsilon + \varepsilon_i - \varepsilon_{\bar{i}}) f_{\alpha \bar{i}}(\varepsilon) [1 - f_{\beta i}(\varepsilon + \varepsilon_i - \varepsilon_{\bar{i}})], \quad (\text{S10c})$$

where $\bar{i} = b/t$ for $i = t/b$. Since the intermediate virtual states acquire a finite lifetime during the tunneling processes, we added a small positive parameter η . We now use the identity

$$f_a(\varepsilon_i) [1 - f_b(\varepsilon_j)] = \frac{1}{2} n_B(\varepsilon_i - \varepsilon_j - \mu_a + \mu_b) [\tanh(\beta(\varepsilon_i - \mu_a)/2) - \tanh(\beta(\varepsilon_j - \mu_b)/2)], \quad (\text{S11})$$

where $n_B(x) = 1/(\exp(\beta x) + 1)$. Here, $\tanh(z)$ can be expressed as

$$\tanh(z) = -\frac{i}{\pi} \left[\Psi\left(\frac{1}{2} + i\frac{z}{\pi}\right) - \Psi\left(\frac{1}{2} - i\frac{z}{\pi}\right) \right], \quad (\text{S12})$$

where $\Psi(z)$ denotes the digamma function. Employing the fact that $\Psi(\frac{1}{2} + i\frac{z}{2\pi})$ has the poles in the upper halfplane at the locations $z = i\pi(1/2 + n)$, where $n \in \mathbb{N}$, while the poles of $\Psi(\frac{1}{2} - i\frac{z}{2\pi})$ are in the lower halfplane at the locations $z = -i\pi(1/2 + n)$, the integrals in Eqs. (S10) can then be easily calculated. In the final stage, we expand the results in powers of η . Those terms scaling as $1/\eta$ are removed since they are indeed sequential tunneling processes and cannot be counted twice. Then, we take the limit $\eta \rightarrow 0$ and find

$$\gamma_{00/bb}^{\alpha b \beta b} = \frac{\beta}{4\pi^2 \hbar} \Gamma_{\alpha b} \Gamma_{\beta b} n_B(\mu_{\beta b} - \mu_{\alpha b}) \Im \left[\Psi^{(1)}\left(\frac{1}{2} + i\beta \frac{\varepsilon_b - \mu_{\alpha b}}{2\pi}\right) - \Psi^{(1)}\left(\frac{1}{2} + i\beta \frac{\varepsilon_b - \mu_{\beta b}}{2\pi}\right) \right], \quad (\text{S13a})$$

$$\begin{aligned} \gamma_{tb}^{\alpha b Lt} &= \frac{\Gamma_{\alpha b} \Gamma_{Lt}}{2\pi \hbar} n_B(\varepsilon_b - \varepsilon_t + \mu_{Lt} - \mu_{\alpha b}) \\ &\times \left\{ \frac{D^2}{D^2 + (\varepsilon_t - \mu_{Lt})^2} \Im \left[\frac{2i(\varepsilon_t - \mu_{Lt})}{D^2 + (\varepsilon_t - \mu_{Lt})^2} \left(\Psi\left(\frac{1}{2} + i\beta \frac{\varepsilon_b - \mu_{\alpha b}}{2\pi}\right) - \Psi\left(\frac{1}{2} + i\beta \frac{\varepsilon_t - \mu_{Lt}}{2\pi}\right) \right) \right. \right. \\ &\quad \left. \left. + \frac{\beta}{2\pi} \left(\Psi^{(1)}\left(\frac{1}{2} + i\beta \frac{\varepsilon_b - \mu_{\alpha b}}{2\pi}\right) - \Psi^{(1)}\left(\frac{1}{2} + i\beta \frac{\varepsilon_t - \mu_{Lt}}{2\pi}\right) \right) \right] \right. \\ &\quad \left. + \frac{1}{D} \Im \left[\frac{D^2}{(\varepsilon_u - \mu_{Lt} + iD)^2} \left(\Psi\left(\frac{1}{2} + \frac{\beta D}{2\pi}\right) + i\beta \frac{\varepsilon_b - \varepsilon_t - \mu_{\alpha b} + \mu_{Lt}}{2\pi} \right) - \Psi\left(\frac{1}{2} + \frac{\beta D}{2\pi}\right) \right] \right\}, \quad (\text{S13b}) \end{aligned}$$

$$\begin{aligned} \gamma_{bt}^{Lt \alpha b} &= \frac{\Gamma_{Lt} \Gamma_{\alpha b}}{2\pi \hbar} n_B(\varepsilon_t - \varepsilon_b + \mu_{\alpha b} - \mu_{Lt}) \\ &\times \left\{ \frac{D^2}{D^2 + (\varepsilon_t - \mu_{Lt})^2} \Im \left[\frac{2i(\varepsilon_t - \mu_{Lt})}{D^2 + (\varepsilon_t - \mu_{Lt})^2} \left(\Psi\left(\frac{1}{2} + i\beta \frac{\varepsilon_t - \mu_{Lt}}{2\pi}\right) - \Psi\left(\frac{1}{2} + i\beta \frac{\varepsilon_b - \mu_{\alpha b}}{2\pi}\right) \right) \right. \right. \\ &\quad \left. \left. + \frac{\beta}{2\pi} \left(\Psi^{(1)}\left(\frac{1}{2} + i\beta \frac{\varepsilon_t - \mu_{Lt}}{2\pi}\right) - \Psi^{(1)}\left(\frac{1}{2} + i\beta \frac{\varepsilon_b - \mu_{\alpha b}}{2\pi}\right) \right) \right] \right. \\ &\quad \left. + \frac{1}{D} \Im \left[\frac{D^2}{(\varepsilon_u - \mu_{Lt} + iD)^2} \left(\Psi\left(\frac{1}{2} + \frac{\beta D}{2\pi}\right) - \Psi\left(\frac{1}{2} + \frac{\beta D}{2\pi} + i\beta \frac{\varepsilon_b - \varepsilon_t - \mu_{\alpha b} + \mu_{Lt}}{2\pi}\right) \right) \right] \right\}, \quad (\text{S13c}) \end{aligned}$$

$$\gamma_{tb}^{\alpha b Rt} = \frac{\beta \Gamma_{\alpha b} \Gamma_{Rt}}{4\pi^2 \hbar} n_B(\varepsilon_b - \varepsilon_t + \mu_{Rt} - \mu_{\alpha b}) \Im \left[\Psi^{(1)}\left(\frac{1}{2} + i\beta \frac{\varepsilon_b - \mu_{\alpha b}}{2\pi}\right) - \Psi^{(1)}\left(\frac{1}{2} + i\beta \frac{\varepsilon_t - \mu_{Rt}}{2\pi}\right) \right], \quad (\text{S13d})$$

$$\gamma_{bt}^{Rt \alpha b} = \frac{\beta \Gamma_{Rt} \Gamma_{\alpha b}}{4\pi^2 \hbar} n_B(\varepsilon_t - \varepsilon_b + \mu_{\alpha b} - \mu_{Rt}) \Im \left[\Psi^{(1)}\left(\frac{1}{2} + i\beta \frac{\varepsilon_t - \mu_{Rt}}{2\pi}\right) - \Psi^{(1)}\left(\frac{1}{2} + i\beta \frac{\varepsilon_b - \mu_{\alpha b}}{2\pi}\right) \right]. \quad (\text{S13e})$$

ELECTROSTATIC MODEL

With the geometry shown in Fig. S1, the electrostatic equations for the charges Q_t and Q_b are given by

$$Q_t = \sum_{\alpha=1}^4 C_{\alpha t}(\phi_t - V_{\alpha}) + C(\phi_t - \phi_b), \quad (\text{S14a})$$

$$Q_b = \sum_{\alpha=1}^4 C_{\alpha b}(\phi_b - V_{\alpha}) + C(\phi_b - \phi_t). \quad (\text{S14b})$$

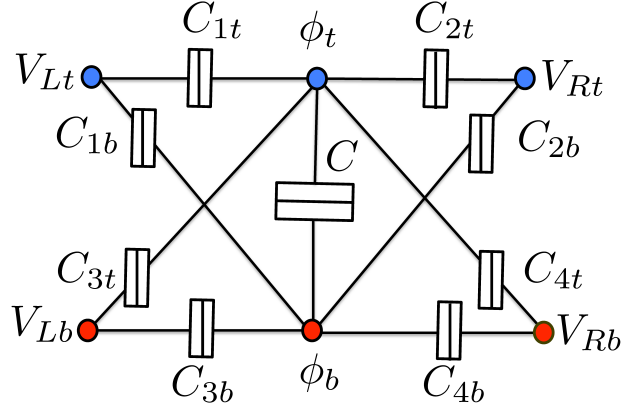


FIG. S1. Electrostatic model for the double quantum dot system.

To shorten the notation, we set $V_1 = V_{Lt}$, $V_2 = V_{Rt}$, $V_3 = V_{Lb}$ and $V_4 = V_{Rb}$. Solving Eq. (S14), we find the internal potentials ϕ_t and ϕ_b

$$\phi_t = \frac{1}{K} \left[\sum_{\alpha} C_{\alpha b} (Q_t + \sum_{\beta} C_{\beta t} V_{\beta}) + C(Q_t + Q_b + \sum_{\alpha} \sum_{i=t/b} C_{\alpha i} V_{\alpha}) \right], \quad (\text{S15a})$$

$$\phi_b = \frac{1}{K} \left[\sum_{\alpha} C_{\alpha t} (Q_b + \sum_{\beta} C_{\beta b} V_{\beta}) + C(Q_t + Q_b + \sum_{\alpha} \sum_{i=t/b} C_{\alpha i} V_{\alpha}) \right], \quad (\text{S15b})$$

where

$$K = \sum_{\alpha} C_{\alpha t} \sum_{\beta} C_{\beta b} + C \sum_{\alpha} \sum_{i=t/b} C_{\alpha i}. \quad (\text{S16})$$

The potential energies with N_t and N_b excess electrons then take the form

$$U_t(N_t, N_b) = \int_0^{eN_t} dQ_t \phi_t(Q_t, Q_b), \quad (\text{S17a})$$

$$U_b(N_t, N_b) = \int_0^{eN_b} dQ_b \phi_b(Q_t, Q_b), \quad (\text{S17b})$$

which become

$$U_t(N_t, N_b) = \frac{eN_t}{2K} \left[\sum_{\alpha} C_{\alpha b} (eN_t + 2 \sum_{\beta} C_{\beta t} V_{\beta}) + C(eN_t + 2eN_b + 2 \sum_{\alpha} \sum_{i=t/b} C_{\alpha i} V_{\alpha}) \right], \quad (\text{S18a})$$

$$U_b(N_t, N_b) = \frac{eN_b}{2K} \left[\sum_{\alpha} C_{\alpha t} (eN_b + 2 \sum_{\beta} C_{\beta b} V_{\beta}) + C(2eN_t + eN_b + 2 \sum_{\alpha} \sum_{i=t/b} C_{\alpha i} V_{\alpha}) \right]. \quad (\text{S18b})$$

In the uncharged case, the electrochemical potential (effective level) of top or bottom dot can be written as

$$\varepsilon_{t0}^{\text{eff}} = E_t - E_0 = \varepsilon_t + U_t(1, 0) - U_t(0, 0), \quad (\text{S19a})$$

$$\varepsilon_{b0}^{\text{eff}} = E_b - E_0 = \varepsilon_b + U_b(0, 1) - U_b(0, 0), \quad (\text{S19b})$$

where E_i is the single-particle kinetic energy plus the internal potential energy. Equation (S19) is the energy required to add one electron into top or bottom dot when both levels are empty:

$$\varepsilon_{t0}^{\text{eff}} = \varepsilon_t + \frac{e}{2K} \left[\sum_{\alpha} C_{\alpha b} (e + 2 \sum_{\beta} C_{\beta t} V_{\beta}) + C (e + 2 \sum_{\alpha} \sum_{i=t/b} C_{\alpha i} V_{\alpha}) \right], \quad (\text{S20a})$$

$$\varepsilon_{b0}^{\text{eff}} = \varepsilon_b + \frac{e}{2K} \left[\sum_{\alpha} C_{\alpha t} (e + 2 \sum_{\beta} C_{\beta b} V_{\beta}) + C (e + 2 \sum_{\alpha} \sum_{i=t/b} C_{\alpha i} V_{\alpha}) \right]. \quad (\text{S20b})$$

The Fermi functions are evaluated at $\varepsilon_{i0}^{\text{eff}} - \mu_{\alpha}$, where $\mu_{\alpha} = E_F + eV_{\alpha}$ with E_F the common Fermi energy:

$$\varepsilon_{t0}^{\text{eff}} - \mu_1 = \varepsilon_t - E_F + \frac{1}{K} \left[\frac{e^2 (\sum_{\alpha} C_{\alpha b} + C)}{2} + e \sum_{\alpha, \beta} C_{\alpha b} C_{\beta t} V_{\beta 1} + e \sum_{\alpha, i} C C_{\alpha i} V_{\alpha 1} \right], \quad (\text{S21a})$$

$$\varepsilon_{t0}^{\text{eff}} - \mu_2 = \varepsilon_t - E_F + \frac{1}{K} \left[\frac{e^2 (\sum_{\alpha} C_{\alpha b} + C)}{2} + e \sum_{\alpha, \beta} C_{\alpha b} C_{\beta t} V_{\beta 2} + e \sum_{\alpha, i} C C_{\alpha i} V_{\alpha 2} \right], \quad (\text{S21b})$$

$$\varepsilon_{b0}^{\text{eff}} - \mu_3 = \varepsilon_b - E_F + \frac{1}{K} \left[\frac{e^2 (\sum_{\alpha} C_{\alpha t} + C)}{2} + e \sum_{\alpha, \beta} C_{\alpha t} C_{\beta b} V_{\beta 3} + e \sum_{\alpha, i} C C_{\alpha i} V_{\alpha 3} \right], \quad (\text{S21c})$$

$$\varepsilon_{b0}^{\text{eff}} - \mu_4 = \varepsilon_b - E_F + \frac{1}{K} \left[\frac{e^2 (\sum_{\alpha} C_{\alpha t} + C)}{2} + e \sum_{\alpha, \beta} C_{\alpha t} C_{\beta b} V_{\beta 4} + e \sum_{\alpha, i} C C_{\alpha i} V_{\alpha 4} \right], \quad (\text{S21d})$$

Here, $V_{\alpha\beta} = V_{\alpha} - V_{\beta}$ and our model is gauge invariant as should be.

For $U \rightarrow \infty$, the doubly occupied state is forbidden, which amounts to taking the limit $C \rightarrow \infty$. We then have

$$\varepsilon_{t0}^{\text{eff}} - \mu_1 = \varepsilon_t - E_F + \frac{e^2}{2C_{\Sigma}} + \frac{e}{C_{\Sigma}} \sum_{\alpha, i} C_{\alpha i} V_{\alpha 1}, \quad (\text{S22a})$$

$$\varepsilon_{t0}^{\text{eff}} - \mu_2 = \varepsilon_t - E_F + \frac{e^2}{2C_{\Sigma}} + \frac{e}{C_{\Sigma}} \sum_{\alpha, i} C_{\alpha i} V_{\alpha 2}, \quad (\text{S22b})$$

$$\varepsilon_{b0}^{\text{eff}} - \mu_3 = \varepsilon_b - E_F + \frac{e^2}{2C_{\Sigma}} + \frac{e}{C_{\Sigma}} \sum_{\alpha, i} C_{\alpha i} V_{\alpha 3}, \quad (\text{S22c})$$

$$\varepsilon_{b0}^{\text{eff}} - \mu_4 = \varepsilon_b - E_F + \frac{e^2}{2C_{\Sigma}} + \frac{e}{C_{\Sigma}} \sum_{\alpha, i} C_{\alpha i} V_{\alpha 4} \quad (\text{S22d})$$

with

$$C_{\Sigma} = \sum_{\alpha, i} C_{\alpha i}. \quad (\text{S23})$$

For the numerical simulations of the main article we use in units of e^2/Γ_0 the values $C_{1t} = 1/202$, $C_{2t} = 1/815$, $C_{3b} = 1/1485$, $C_{4b} = 1/177$ and $C_{1b} = C_{2b} = C_{3t} = C_{4t} = 0$.